



Probing Supermassive Black Hole Seed Scenarios with Gravitational-wave Measurements

John Ellis^{1,2,3}, Malcolm Fairbairn¹, Juan Urrutia^{3,4}, and Ville Vaskonen^{3,5,6}

¹ King's College London, Strand, London WC2R 2LS, UK; malcolm.fairbairn@kcl.ac.uk, john.ellis@cern.ch

² Theoretical Physics Department, CERN, Geneva, Switzerland

³ Keemilise ja Bioloogilise Füüsika Instituut, Rävåla pst. 10, 10143 Tallinn, Estonia; juan.urrutia@kbfi.ee, ville.vaskonen@pd.infn.it

⁴ Department of Cybernetics, Tallinn University of Technology, Akadeemia tee 21, 12618 Tallinn, Estonia

⁵ Dipartimento di Fisica e Astronomia, Università degli Studi di Padova, Via Marzolo 8, 35131 Padova, Italy

⁶ Istituto Nazionale di Fisica Nucleare, Sezione di Padova, Via Marzolo 8, 35131 Padova, Italy

Received 2024 January 17; revised 2024 February 8; accepted 2024 February 9; published 2024 March 11

Abstract

The process whereby the supermassive black holes (SMBHs) populating the centers of galaxies have been assembled remains to be established, with the relative importance of seeds provided by collapsed Population III stars, black holes formed in nuclear star clusters via repeated mergers, or direct collapses of protogalactic disks yet to be determined. In this paper we study the prospects for casting light on this issue by future measurements of gravitational waves emitted during the inspirals and mergers of pairs of intermediate-mass black holes (IMBHs), discussing in particular the roles of prospective measurements by LISA and the proposed atom interferometers AION and AEDGE. We find that the expected number of detectable IMBH binaries is $\mathcal{O}(100)$ for LISA and AEDGE and $\mathcal{O}(10)$ for AION in low-mass seeds scenarios and goes down to $\mathcal{O}(10)$ for LISA and below one for AEDGE and AION in high-mass seed scenarios. This allows all of these observatories to probe the parameters of the seed model, in particular, if at least a fraction of the SMBHs arises from a low-mass seed population. We also show that the measurement accuracy of the binary parameters is, in general, best for AEDGE, which sees very precisely the merger of the binary.

Unified Astronomy Thesaurus concepts: [Intermediate-mass black holes \(816\)](#); [Gravitational waves \(678\)](#); [Cosmology \(343\)](#); [Supermassive black holes \(1663\)](#)

1. Introduction

Most galaxies contain supermassive black holes (SMBHs) heavier than $10^6 M_\odot$ (Kormendy & Ho 2013), and the existence of black holes (BHs) with masses between a few and $\sim 80 M_\odot$ has been established by observations of X-ray binaries (Remillard & McClintock 2006) and by the measurements of gravitational waves (GWs) with frequencies ~ 100 Hz emitted during their mergers (Abbott et al. 2019, 2021a, 2021b). Various other observations point to the existence of intermediate-mass black holes (IMBHs) with masses in the range 10^4 – $10^6 M_\odot$, but their mass function and redshift distribution is known only very poorly (Greene et al. 2020). This lack of information about IMBHs impedes our understanding of how SMBHs have been assembled (Reines 2022).

The main possibilities for seeding SMBH assembly include collapsed Population III stars (Madau & Rees 2001; Bromm & Loeb 2003), BHs formed in nuclear star clusters via repeated mergers (Atakan Gurkan et al. 2004; Portegies Zwart et al. 2004; Natarajan 2021), or direct collapses of protogalactic disks in which fragmentation is suppressed (Sesana et al. 2004; Begelman et al. 2006; Mayer et al. 2007; Volonteri et al. 2008; Tanaka & Li 2014; Inayoshi et al. 2015; Izquierdo-Villalba et al. 2023). All of these mechanisms are capable of reproducing the properties of the observed SMBH population for suitable values of assembly parameters, such as accretion rates, but can differ significantly in their predictions for the

spectrum of IMBH mergers at different redshifts; see Volonteri et al. (2021) for an overview. Signatures of these mechanisms may include either light seeds, with masses $\sim 10^2$ – $10^3 M_\odot$, or heavy seeds, with masses $\sim 10^4$ – $10^5 M_\odot$, at $z \lesssim 10$. These are currently unconstrained by data, but can in principle be probed by future GW and other measurements (Sesana et al. 2011; Hartwig et al. 2016; Krolik et al. 2019; Mangiagli et al. 2020; Volonteri et al. 2020; Haidar et al. 2022; Dong-Páez et al. 2023).

The purpose of this paper is to investigate what progress can be made in distinguishing between the SMBH assembly scenarios with planned future GW experiments at frequencies larger than 0.1 mHz in light of recent data on nHz GWs from pulsar timing array (PTA) experiments, highlighting the potential capabilities of atom interferometers. Whereas PTAs are sensitive to the early inspiralling phase of the SMBHs heavier than $10^9 M_\odot$, the future GW experiments will probe directly the infalls and mergers of binaries lighter than $10^7 M_\odot$.

NANOGrav (Agazie et al. 2023a) and other PTA experiments (Antoniadis et al. 2023a; Xu et al. 2023; Zic et al. 2023) have recently reported the observation of a stochastic background of GWs at frequencies in the nHz range, for which the most conservative astrophysical interpretation is that binary systems of SMBHs are emitting them with masses $\sim 10^9 M_\odot$ (Agazie et al. 2023b, 2023c; Antoniadis et al. 2023b; Ellis et al. 2023). Naive extrapolation of binary merger models to lower BH masses suggests that GWs from IMBH binaries may be observable at higher frequencies between 0.1 mHz and 1 Hz, for example by the LISA spaceborne laser interferometer experiment or atom interferometer experiments (Ellis et al. 2024). In principle, there are two regimes where the formation

channels of the SMBHs may be distinguished. Either at $z \gtrsim 7$ when the seeds are assembling and scaling relations are not that strong (Treister et al. 2013; Ricarte & Natarajan 2018a), or by observing the low-mass occupation fraction of dwarf galaxies and dark matter halos at more recent times (Ricarte & Natarajan 2018b; Volonteri et al. 2021). The extrapolation to higher frequencies of a model that can fit the NANOGrav background (Ellis et al. 2023) predicts that the majority of detectable binaries will be at $z < 7$, so the focus of this study is to constrain the latter. Our work complements analogous studies that have been performed with electromagnetic observations of active galactic nuclei (AGNs; Kelly & Shen 2013; Miller et al. 2015; Gallo & Sesana 2019; Chadayammuri et al. 2023).

To extend these observations to the GW spectrum and establish a multimessenger signal, we estimate how well the spaceborne laser interferometer experiment LISA (Amaro-Seoane et al. 2017) and the atom interferometers AION-1 km (Badurina et al. 2020, 2021) and AEDGE (El-Neaj et al. 2020; Badurina et al. 2021) could recover the occupation fraction and the weight of the different channels contributing to the formation of the SMBHs.⁷ Our approach is to generate populations of the IMBH binaries, estimate how well the binary parameters could be recovered, and then construct posteriors for the parameters of the merger rate. To extend the deduced merger rate from the NANOGrav observations, we assume that the scaling relation extends to lower masses in a light-seed scenario. Although there is evidence for this assumption (Baldassare et al. 2020), there is no consensus among simulations and semianalytical models (Fontanot et al. 2015). However, under this assumption, we predict that laser and atom interferometers will be to place new and competitive constraints after their first years of observation, shedding light on the origin of SMBHs.

2. Model

We use the extended Press–Schechter formalism (Press & Schechter 1974; Bond et al. 1991; Lacey & Cole 1993) to estimate the rate R_h of coalescences of galactic halos of masses $M_{1,2}$. Assuming conservatively that each of the halos includes at most one BH and that the BHs merge with the halos with probability p_{BH} (Ellis et al. 2023), the merger rate of BHs can be written as

$$\frac{dR_{\text{BH}}(p_{\text{BH}}, \theta)}{dm_1 dm_2} \approx p_{\text{BH}} \int dM_1 dM_2 \times \frac{dR_h}{dM_1 dM_2} \prod_{j=1,2} p_{\text{occ}}(m_j | M_j, z, \theta), \quad (1)$$

where $p_{\text{occ}}(m_{\text{BH}} | M_v, z, \theta)$ is the occupation fraction of BHs of mass m_{BH} in halos of mass M_v at redshift z , and the mechanisms for SMBH formation are characterized by a set of parameters θ . We fix the value of the merging efficiency p_{BH} to 0.84, which corresponds to the best fit of the SGWB measured by the NANOGrav collaboration (Ellis et al. 2024). This fit was obtained by including environmental effects on the binary evolution. Such effects are preferred by the fit but will not affect the binaries at the frequencies considered in this study.

We model the occupation fraction $p_{\text{occ}}(m_{\text{BH}} | M_v, z, \theta)$ by a sum over different SMBH seed channels:

$$p_{\text{occ}}(m_{\text{BH}} | M_v, z, \theta) = \sum_j \frac{p_j(m_{\text{BH}}, \theta_j)}{\sqrt{2\pi} m_{\text{BH}} \sigma} \exp\left[-\frac{\ln(m_{\text{BH}}/\bar{m})^2}{2\sigma^2}\right], \quad (2)$$

where the lognormal distribution parameterizes the halo mass–BH mass relation and p_j parameterizes the low-mass cut of the massive BH population. We compute the latter by using the observed halo mass–stellar mass relation $M_*(M_v)$ (Girelli et al. 2020), the mean stellar mass–BH mass relation obtained from observations of inactive galaxies⁸ (Kormendy & Ho 2013; Reines & Volonteri 2015), $\log_{10}(\bar{m}/M_\odot) = 8.95 + 1.4 \log_{10}(M_*/10^{11} M_\odot)$, and the observed scatter of $\sigma = 1.1$ in the latter.⁹

At low redshifts, $z \lesssim 7$, different SMBH seed scenarios are reflected in differences in the low-mass end of the occupation fraction. This is accounted for by the functions $p_j(m_{\text{BH}}, \theta_j)$ for which we consider the following parametric form:

$$p_j(m_{\text{BH}}, \theta_j) = \frac{f_j}{2} \left(1 + \text{erf} \left[\frac{\log_{10}(m_{\text{BH}}/m_{\text{cut},j})}{w_j} \right] \right) \quad (3)$$

with the parameters $\theta_j = (f_j, m_{\text{cut},j}, w_j)$, where f_j is the fraction of SMBHs produced by a given mechanism j , $m_{\text{cut},j}$ characterizes a cut on the minimal SMBH mass, and w_j is the spread with which the minimal-mass cut is applied.¹⁰ We fix $\sum_j f_j = 1$. The function p_j is shown in the left panel of Figure 1 for different values of m_{cut} and w . In the following analysis, we consider two cases: (1) a one-component model where the SMBH population arises from one seed population and (2) a two-component model that includes a population arising from light seeds, e.g., BH remnants of Population III stars, and a population arising from heavy seeds, e.g., BH nuclei of protogalaxies. We show an example of the occupation fraction p_{occ} in the latter case in the right panel of Figure 1.¹¹

We emphasize that the above estimate of the BH merger rate is subject to various uncertainties. In particular, we neglect the additional delays related to the binary evolution following a halo merger (Hao et al. 2024) as well as possible difficulties for the SMBH to shrink to the galactic cores in dwarf galaxies (Dayal et al. 2020; Dunn et al. 2020), and we extrapolate the halo mass–BH mass relation to much lower masses than where it is currently measured. However, since our goal is mainly to illustrate and compare the capabilities of LISA, AION, and AEDGE, a detailed discussion of overall uncertainties is beyond the scope of this work.

⁸ Another measurement of the stellar mass–BH mass relation comes from AGN observations. As discussed in Ellis et al. (2024), this relation might not reflect the full low- z massive BH population but only its low-mass tail.

⁹ Notice that we use the lognormal distribution in Equation (2), so this scatter corresponds to 0.47 dex as in Reines & Volonteri (2015).

¹⁰ A qualitatively similar parameterization of the occupation fraction was adopted in Miller et al. (2015) and in Chadayammuri et al. (2023) for studies of SMBH seed models with electromagnetic observations of AGNs.

¹¹ There may be other BH binary populations that can complicate the searches of the population related to the assembly of SMBHs. In particular, IMBH binaries may form in dense stellar clusters (Rasskazov et al. 2020; Fragione et al. 2022). The merger rate of this binary population, however, depends differently on redshift than the merger rate we consider and may become relevant only at $z \lesssim 1$.

⁷ See also the related discussion of the capability of the proposed TianQin experiment in Wang et al. (2019).

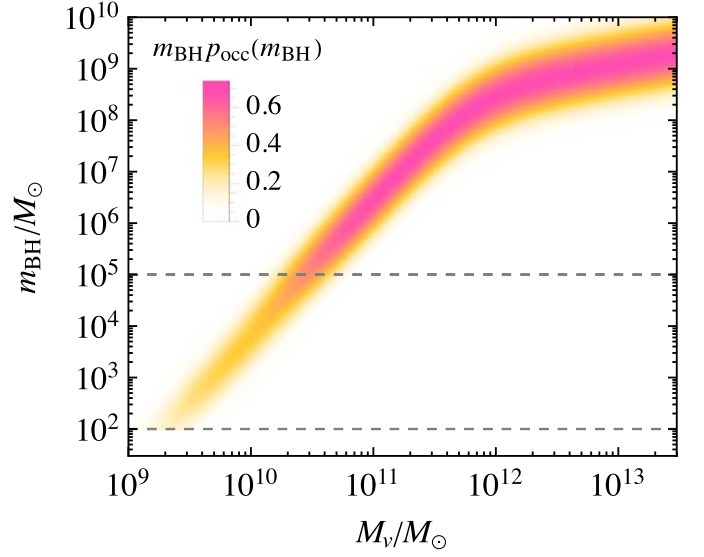
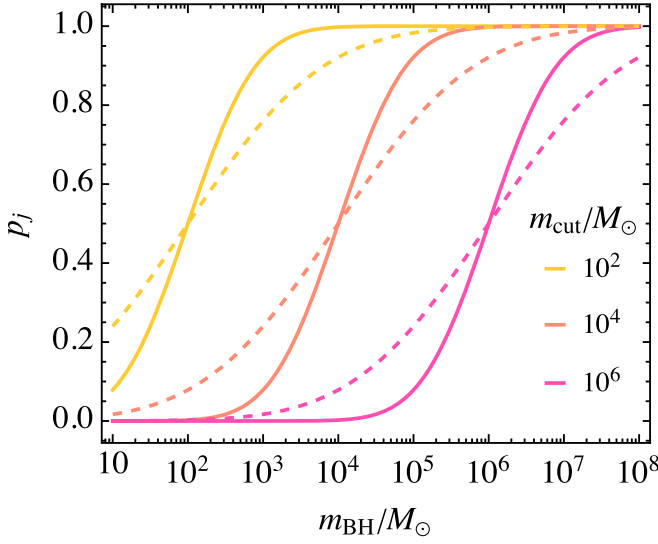


Figure 1. Left panel: the low-mass cut on the massive BH population for different values of m_{cut} , for $w = 1$ (solid) and $w = 2$ (dashed). Right panel: the halo mass–BH mass relation. The color coding shows the BH occupation fraction p_{occ} as a function of the halo mass M_v , and the BH mass m_{BH} for a scenario with $f_1 = f_2 = 0.5$, $w_1 = w_2 = 1$, $m_{\text{cut},1} = 100 M_{\odot}$, and $m_{\text{cut},2} = 10^5 M_{\odot}$.

3. GW Data Analysis

For each specific SMBH formation model, characterized by the parameters θ , we generate n Monte Carlo (MC) realizations of the expected binary populations using Equation (1). The number of binaries N_j in any given MC realization follows a Poisson distribution whose mean is the expected number $\bar{N}(\theta)$ of detectable binaries during one year of observation. The latter is given by

$$\bar{N}(\theta) = \int_0^{\infty} d\tau \int d\lambda(\theta, \mathbf{x}) p_{\text{det}}[(S/N_c)/(S/N(\mathbf{x}, \tau))], \quad (4)$$

where $S/N(\mathbf{x})$ is the signal-to-noise ratio of the GW signal from a binary with parameters \mathbf{x} in an optimal source-detector system for a given GW detector, p_{det} is the detection probability that accounts for the source location and orientation (Finn & Chernoff 1993; Gerosa et al. 2019), and $S/N_c = 8$.

To characterize how well the parameters of the formation mechanism can be measured, we compute the likelihood for each of the MC realizations (Mandel et al. 2019; Hütsi et al. 2021):

$$\ell_j(\theta) \propto e^{-\bar{N}(\theta)} \prod_{i=1}^{N_j} \int d\lambda(\theta, \mathbf{x}) P_i(\mathbf{x}_i|\mathbf{x}), \quad (5)$$

where $\mathbf{x}_i = (m_{1,i}, m_{2,i}, z_i)$ are the parameters of the i th binary in the generated population, $\mathbf{x} = (m_1, m_2, z)$ are the integration variables and

$$d\lambda(\theta, \mathbf{x}) \equiv \frac{1}{1+z} \frac{dV_c}{dz} \frac{dR_{\text{BH}}(p_{\text{BH}}, \theta)}{dm_1 dm_2} dm_1 dm_2 dz. \quad (6)$$

The distributions $p_i(\mathbf{x}_i|\mathbf{x})$ account for the accuracy with which the parameters of the binary i can be measured. We assume that $p_i(\mathbf{x}_i|\mathbf{x})$ follows a multivariate Gaussian distribution centered around the true values \mathbf{x}_i , and estimate the covariance matrix from the Fisher information, $\Sigma_{kl}(\mathbf{x}_i) = \Gamma_{kl}^{-1}(\mathbf{x}_i)$. Finally, we compute the expected likelihood

as

$$\ell(\theta) = \frac{1}{n} \sum_{j=1}^n \ell_j(\theta) \quad (7)$$

and use that to estimate the expected accuracy at which the model parameters θ can be measured.

We express the optimal S/N and the Fisher matrix $\Gamma_{kl}(\mathbf{x})$ of a signal as (Poisson & Will 1995)

$$\begin{aligned} S/N(\mathbf{x}) &= \sqrt{\langle \tilde{h}(\mathbf{x}) | \tilde{h}(\mathbf{x}) \rangle}, \\ \Gamma_{kl}(\mathbf{x}) &= \langle \partial_k \tilde{h}(\mathbf{x}) | \partial_l \tilde{h}(\mathbf{x}) \rangle, \end{aligned} \quad (8)$$

by defining the inner product of two complex functions $a(f)$ and $b(f)$ as

$$\langle a(f) | b(f) \rangle = 2 \int_{f(\tau)}^{f(\tau-T)} df \frac{a^*(f)b(f) + b^*(f)a(f)}{S_n(f)}, \quad (9)$$

where \mathcal{T} denotes the observation time and $S_n(f)$ is the noise power spectral density of the considered GW experiment. The partial derivatives in the Fisher matrix are taken with respect to the parameters of the template. We take into account the binary component masses m_1 and m_2 , its redshift z , the phase of the GW signals ϕ_c , and its coalescence time τ , but not the binary sky location or inclination, over which we simply average. To estimate the Fourier transform of the GW strain, $\tilde{h}(\mathbf{x})$, we use the inspiral-merger-ringdown template (Ajith et al. 2008).

4. Results

4.1. Binary Population

We perform the analysis for LISA, AEDGE, and AION-1 km. As can be seen in the left panel of Figure 2, LISA is expected to observe more binaries than AEDGE. For low-mass seed scenarios, this difference is small but it grows with m_{cut} implying that LISA will perform much better than AEDGE for heavy-seed scenarios. In particular, the expected number of binaries observable with AEDGE is less than one for heavy-

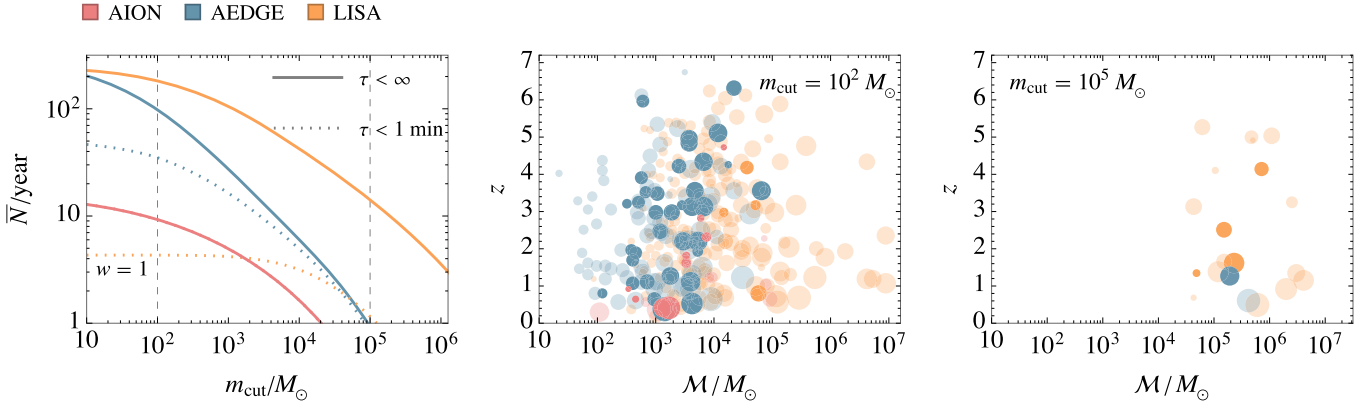


Figure 2. Left panel: the expected numbers of binaries detectable by AION-1 km, AEDGE, and LISA during 1 yr of observation, as functions of m_{cut} . The solid curves show all detectable binaries whereas the dotted curves show only those for which the last 1 minute of the merger is seen. Middle and right panels: explicit examples of the detectable binaries for a light-seed and a heavy-seed scenario. The sizes of the dots are $\propto \ln[S/N]$ with the minimum size corresponding to $S/N = 10^4$ and the maximal to $S/N = 10$. The darker dots correspond to binaries for which the last 1 minute of the merger is seen.

seed scenarios with $m_{\text{cut}} > 10^5 M_{\odot}$.¹² For Figure 2 we have fixed the width of the mass cut to $w = 1$, but we have checked that small changes to w do not alter significantly these results. Focusing on binaries that can be observed within 1 minute of the merger, the number of events for LISA is reduced to only approximately five events for the light-seed case. In the heavy-seed case, LISA will not see the last 1 minute of the binaries if $m_{\text{cut}} > 10^5 M_{\odot}$. On the other hand, AEDGE would detect most of the binaries until within 1 minute of the merger, except for those with $M_c \lesssim 100 M_{\odot}$. AION-1 km has a similar range to AEDGE but, because it has less sensitivity, the number of events is decreased to around 10 if $m_{\text{cut}} \sim 10^2 M_{\odot}$ and further reduced to one event on average for $2 \times 10^4 M_{\odot}$.

An explicit realization of the binary population in a light-seed scenario with ($m_{\text{cut}} = 10^2 M_{\odot}$) is shown in the middle panel of Figure 2, and in a heavy-seed scenario with ($m_{\text{cut}} = 10^5 M_{\odot}$) in the right panel of Figure 2. We see that AEDGE and, to a lesser extent, AION-1 km will probe IMBH binaries over a range of masses that are too light for LISA, covering the mass range covered by terrestrial laser interferometers from $M_c < 100 M_{\odot}$ to $\sim 10^4 M_{\odot}$. LISA, as expected, will probe heavier binaries up to $M_c \sim 10^7 M_{\odot}$. The types of events each experiment can detect are quite different. Considering the final stages within 1 minute of a merger, AEDGE binaries can explore the range $M \in (10^2 - 10^4) M_{\odot}$ out to redshifts $z \sim 7$. LISA, on the other hand, observes only the last minutes of heavier binaries with $M \in (10^4 - 10^6) M_{\odot}$ and $z \lesssim 4$. Finally, AION-1 km will detect a handful of events for $m_{\text{cut}} < 10^4 M_{\odot}$, at low redshifts, $z < 4$, and mainly in the $(10^3 - 10^4) M_{\odot}$ mass range, mostly in the last moments before the merger.

4.2. Binary Parameters

In Figure 3 we display the accuracies with which LISA, AEDGE, and AION-1 km can measure the binary parameters for two representative choices of the binary component masses, a lighter binary with $(m_1, m_2) = (500, 300) M_{\odot}$ (upper panels)

and a heavier binary with $(m_1, m_2) = (10^4, 5 \times 10^4) M_{\odot}$ (lower panels), as functions of the binary redshift z (left panels) and the time to merge τ (right panels). In general, the measurement accuracy of the binary parameters m_1 , m_2 , and z are similar, and the measurement accuracy is best with AEDGE. The lighter binary enters the AION/AEDGE sensitivity band about a day before the merger. Consequently, the binary is not observable for AION/AEDGE if its coalescence time at the beginning of the experiment is longer than the observation time ($T = 1$ yr). LISA instead sees only the inspiralling part until less than 1 day from the merger and can see binaries whose coalescence time is $\tau \lesssim 10$ yr. The heavier binary is seen with AION/AEDGE for an even shorter time, but since the signal is strong the measurement accuracy is very good. In this case, also LISA sees the merger but the measurement with AEDGE is still more accurate unless the redshift of the binary is high, $z \gtrsim 4$, or its coalescence time is longer than the observation time.

For many binaries, the measurement accuracy with AEDGE or LISA is excellent. The probability distributions of the binary parameters can then be approximated by delta functions in the computation of the likelihood Equation (5) so that the integrals over the binary parameters become trivial because the merger rate is essentially constant over such small parameter ranges. This reduces significantly the computational time for the likelihood. We adopt the delta-function approximation when all binary parameters are measured with better than 10% accuracy.

4.3. Seed Scenarios

To estimate how accurately m_{cut} could be measured with 1 yr data samples, we have generated $n = 20$ realizations of the detectable binary populations for a given value of m_{cut} considering a single SMBH seed population. The left panel of Figure 4 shows on the vertical axis the 95% confidence level (CL) ranges of m_{cut} estimates for $m_{\text{cut}} \in [10^2, 10^6] M_{\odot}$ and taking a flat prior for $\log m_{\text{cut}}$ over the range $m_{\text{cut}} \in [10^2, 10^6] M_{\odot}$. The solid and dashed curves correspond to $w = 1$ and $w = 2$ and show that the measurement accuracy of m_{cut} in these two cases is very similar. We see that the seed mass is best recovered with LISA with a small uncertainty of a factor ~ 2 . For $m_{\text{cut}} \lesssim 10^3 M_{\odot}$ the accuracy with AEDGE is similar to LISA, but the 95% CL range for AEDGE grows for heavier masses. When $m_{\text{cut}} \gtrsim 10^5 M_{\odot}$, only a lower bound is obtained with AEDGE because the expected number of detectable

¹² We have cut the AEDGE sensitivity at 0.01 Hz. Depending on the orbit of the satellites, the Newtonian gravity backgrounds may affect the sensitivity at frequencies below that (Hogan et al. 2011). If these backgrounds do not affect the sensitivity, the expected number of binaries for AEDGE will increase significantly, especially in the heavy-seed scenarios. For AION-1 km we have considered the low-noise model (Badurina et al. 2023).

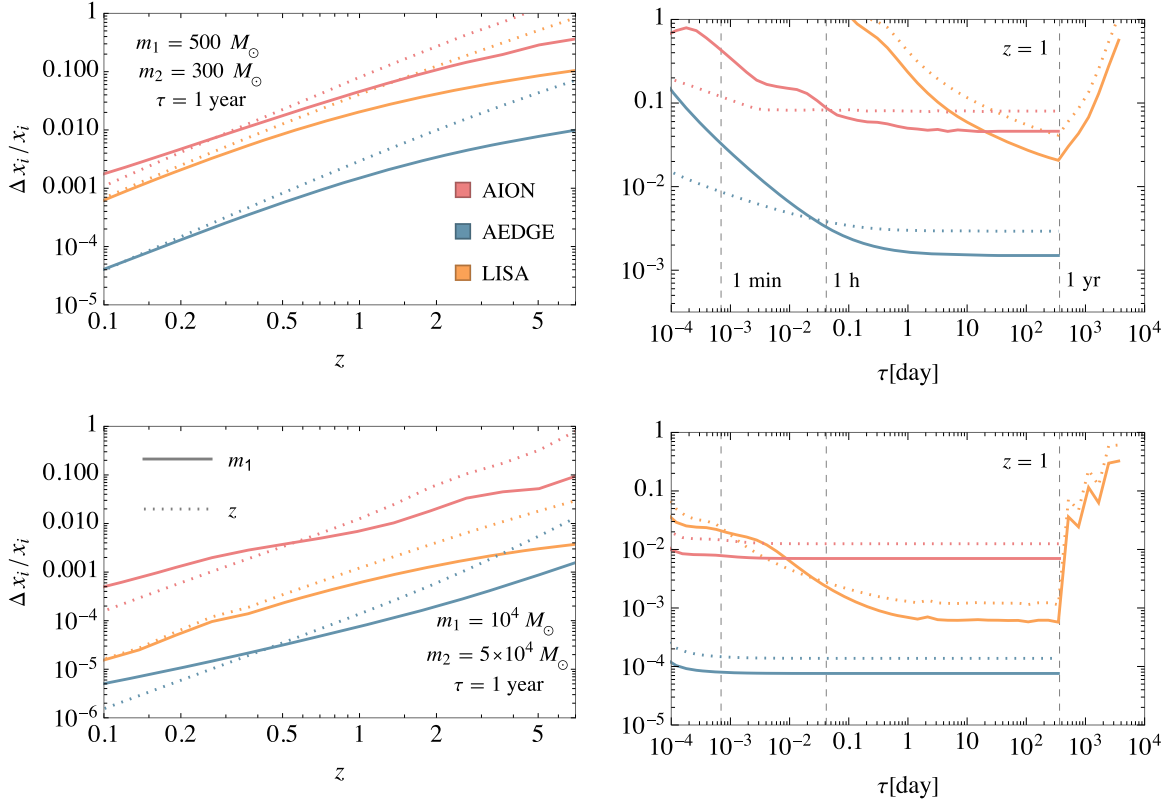


Figure 3. Measurement accuracies for the binary parameters: the upper and lower panels correspond to two binaries whose component masses are fixed. In the left panels, the binary is observed for the last 1 yr and the errors are shown as a function of its redshift. In the right panels, $z = 1$ and the errors are shown as a function of the binary coalescence time at the beginning of a 1 yr observation. The errors for the masses of both BHs are almost the same.

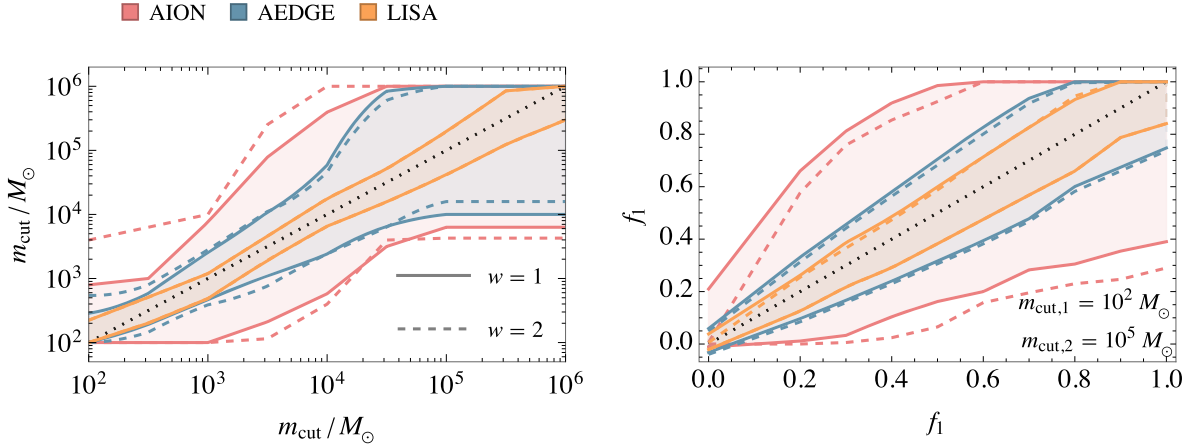


Figure 4. Left panel: the 95% CL accuracy with which LISA, AEDGE, and AION-1 km could measure m_{cut} over the range $[10^2, 10^6] M_{\odot}$. Right panel: the 95% CL accuracy with which LISA, AEDGE, and AION-1 km could measure the fraction of light seeds, f_1 , assuming an input mixture of seeds with masses 10^2 and $10^5 M_{\odot}$ and $f_2 = 1 - f_1$. The solid and dashed curves in both panels correspond, respectively, to $w = 1$ and $w = 2$.

events is less than one in the heavy-seed scenarios. On the other hand, already AION-1 km could measure $m_{\text{cut}} \lesssim 3 \times 10^4 M_{\odot}$ within 1 order of magnitude at 95% CL and could place a 95% CL lower bound of $m_{\text{cut}} \gtrsim 4 \times 10^3 M_{\odot}$ if $m_{\text{cut}} \gtrsim 3 \times 10^4 M_{\odot}$.

In the right panel of Figure 4, we have considered the possibility that there are two different SMBH seed populations, a light one with $m_{\text{cut},1} = 100 M_{\odot}$, and a heavy one with $m_{\text{cut},2} = 10^5 M_{\odot}$. We have again generated $n = 20$ realizations of the detectable binary populations for a given value of f_1 with $f_2 = 1 - f_1$. In the right panel of Figure 4, we show how accurately f_1 can be recovered at the 95% CL. We see that

LISA could measure f_1 with an accuracy $\sim 10\%$, whereas AEDGE could measure f_{light} with an accuracy $\sim 10\%$ – 20% . AION-1 km has a much bigger uncertainty but it would be precise enough that it can differentiate at the 95% CL a pure light-seed from a pure heavy-seed scenario.

For the right panel of Figure 4, we have assumed delta-function priors on $m_{\text{cut},1}$ and $m_{\text{cut},2}$ that might be theoretically motivated. Instead, in Figure 5, we consider a benchmark case with $m_1 = 10^2 M_{\odot}$, $m_2 = 10^5 M_{\odot}$, and $f_1 = f_2 = 0.5$, and show the one- and two-dimensional posteriors for their measurements with AION-1 km (top panel), AEDGE (middle panel), and LISA (bottom panel) assuming the log-uniform priors

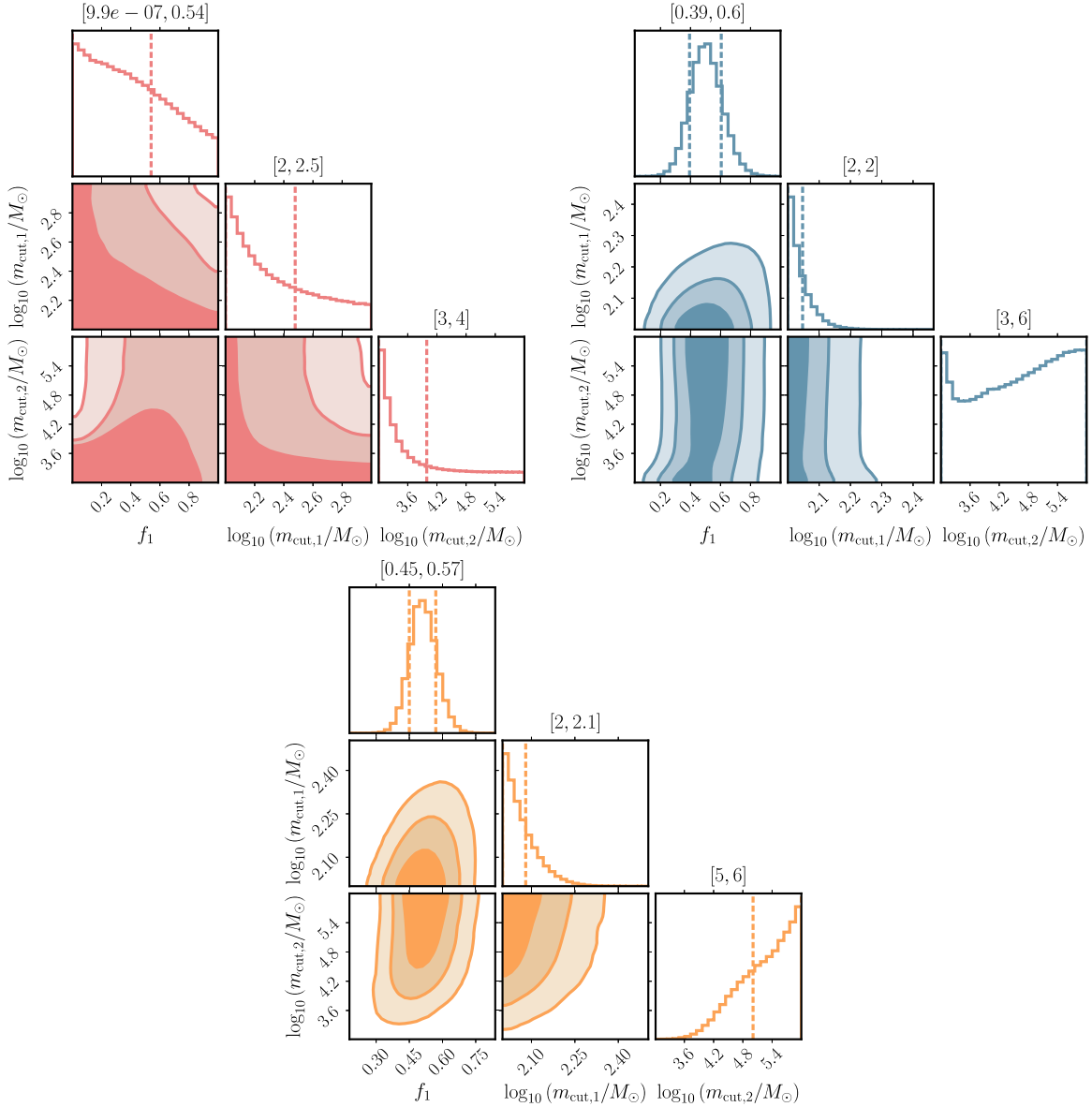


Figure 5. The one- and two-dimensional posteriors of the merger rate parameters (f_1 , $m_{\text{cut},1}$, $m_{\text{cut},2}$) for a two-component seed model with $m_{\text{cut},1} = 10^2 M_{\odot}$, $m_{\text{cut},2} = 10^5 M_{\odot}$ and $f_1 = 0.5$ for AION-1 km (top panel), AEDGE (middle panel), and LISA (bottom panel). The contours enclose the 68%, 95%, and 99% CL regions and the dashed vertical lines show the 68% CL ranges in the marginalized posteriors.

$2 < \log_{10}(m_{\text{cut},1}/M_{\odot}) < 3$ and $3 < \log_{10}(m_{\text{cut},2}/M_{\odot}) < 6$ for the cutoff masses. For simplicity, we keep $w_1 = w_2 = 1$ fixed. We see that AION-1 km provides a good estimate of $m_{\text{cut},1}$, but provides only limited information on $m_{\text{cut},2}$ and f_1 . If we would take the prior $m_{\text{cut},2} \gtrsim 2 \times 10^4 M_{\odot}$, then we would reproduce the lower bound on f_1 with AION-1 km seen in the right panel of Figure 4. On the other hand, AEDGE provides good estimates of both $m_{\text{cut},1}$ and f_1 but also does not constrain $m_{\text{cut},2}$ significantly while LISA not only provides good estimates of both $m_{\text{cut},1}$ and f_1 but also constrains $m_{\text{cut},2}$ significantly. The marginalized posteriors of f_1 for AEDGE and LISA roughly match to the results shown in the right panel of Figure 4.

5. Conclusions

We have described in this paper the capabilities of the planned spaceborne laser interferometer LISA and the proposed atom interferometers AEDGE and AION-1 km to

observe mergers of intermediate-mass BHs, measure their parameters, and discriminate between different seed scenarios for the assembly of SMBHs. We have considered the extended Press–Schechter to model the coalescences of galactic halos and estimate a rate for mergers of SMBHs that is compatible with the PTA signals for GWs in the nHz range. We have extrapolated this model to different SMBH seed scenarios by parameterizing the low-mass cutoff of the massive BH population. Using this parameterization, we have estimated the possible rates for IMBH mergers and assessed their detectability and measurability.

We have found that, although LISA has a high rate for observing the early infall stages of IMBH binaries for all the masses studied, this detector loses many binaries as the merger time approaches. Both AEDGE and AION-1 km have higher rates than LISA for detections within 1 minute of the merger. We have shown that AEDGE has the best perspectives for

detecting mergers of IMBHs weighing $\lesssim 10^4 M_\odot$ whereas LISA has better perspectives for IMBHs weighing $\gtrsim 10^5 M_\odot$. The better detection rates translate into smaller uncertainties in the measurements by AEDGE of binary parameters for IMBHs weighing $\lesssim 10^5 M_\odot$.




We have estimated the accuracy with which a lower cutoff on the BH seed mass, m_{cut} could be extracted from the prospective GW data. We find that both LISA and AEDGE could determine m_{cut} with precision $\lesssim 20\%$ if $m_{\text{cut}} \lesssim 10^4 M_\odot$, whereas LISA could determine m_{cut} with better precision than AEDGE if $m_{\text{cut}} \gtrsim 10^4 M_\odot$. We also find that both LISA and AEDGE have interesting capabilities for distinguishing between scenarios with different mixtures of seeds with 10^2 and $10^5 M_\odot$. AION-1 km could also provide some information, particularly in scenarios with a population of low-mass seeds.

Our results indicate that the spaceborne laser interferometer LISA and atom interferometers AEDGE and AION-1 km have interesting and complementary capabilities for measuring IMBH mergers and distinguishing between different seed scenarios for the assembly of SMBHs. We should emphasize that our study has been exploratory and should be complemented by an improved modeling of the SMBH seed scenarios and more detailed studies of the instrumental capabilities of GW interferometers. It would also be interesting to extend the analysis to assess the prospects for multimessenger observations and study the prospects for measuring higher-order multipoles of the GW signals that would allow, for example, for new probes of strong gravity.

Acknowledgments

The work of J.E. was supported by the United Kingdom STFC grants ST/X000753/1 and ST/T00679X/1, and that of M.F. was also supported by the United Kingdom STFC grant ST/X000753/1. The work of J.U. and V.V. was supported by European Regional Development Fund through the CoE program grant TK202 and by the Estonian Research Council grant PRG803. The work of V.V. was also partially supported by the European Union's Horizon Europe research and innovation program under the Marie Skłodowska-Curie grant agreement No. 101065736.

ORCID iDs

John Ellis  <https://orcid.org/0000-0002-7399-0813>
 Malcolm Fairbairn  <https://orcid.org/0000-0002-0566-4127>
 Juan Urrutia  <https://orcid.org/0000-0002-6035-6610>
 Ville Vaskonen  <https://orcid.org/0000-0003-0003-2259>

References

Abbott, B. P., Abbott, R., Abbott, T. D., et al. 2019, *PhRvX*, 9, 031040
 Abbott, R., Abbott, T. D., Abraham, S., et al. 2021a, *PhRvX*, 11, 021053
 Abbott, R., Abbott, T. D., Acernese, F., et al. 2021b, *PhRvX*, 13, 011048
 Agazie, G., Anumarlapudi, A., Archibald, A. M., et al. 2023a, *ApJL*, 951, L8
 Agazie, G., Anumarlapudi, A., Archibald, A. M., et al. 2023b, *ApJL*, 952, L37
 Agazie, G., Anumarlapudi, A., Archibald, A. M., et al. 2023c, *ApJL*, 951, L50
 Ajith, P., Babak, S., Chen, Y., et al. 2008, *PhRvD*, 77, 104017

Amaro-Seoane, P., Audley, H., Babak, S., et al. 2017, arXiv:1702.00786
 Antoniadis, J., Arumugam, P., Arumugam, S., et al. 2023b, arXiv:2306.16227
 Antoniadis, J., Babak, S., Bak Nielsen, A.-S., et al. 2023a, *A&A*, 678, A48
 Atakan Gurkan, M., Freitag, M., & Rasio, F. A. 2004, *ApJ*, 604, 632
 Badurina, L., Bentine, E., Blas, D., et al. 2020, *JCAP*, 05, 011
 Badurina, L., Buchmueller, O., Ellis, J., et al. 2021, *RSPTA*, 380, 20210060
 Badurina, L., Gibson, V., McCabe, C., & Mitchell, J. 2023, *PhRvD*, 107, 055002
 Baldassare, V. F., Dickey, C., Geha, M., & Reines, A. E. 2020, *ApJ*, 898, L3
 Begelman, M. C., Volonteri, M., & Rees, M. J. 2006, *MNRAS*, 370, 289
 Bond, J. R., Cole, S., Efstathiou, G., & Kaiser, N. 1991, *ApJ*, 379, 440
 Bromm, V., & Loeb, A. 2003, *ApJ*, 596, 34
 Chadayammuri, U., Bogdan, A., Ricarte, A., & Natarajan, P. 2023, *ApJ*, 946, 51
 Dayal, P., Volonteri, M., Choudhury, T. R., et al. 2020, *MNRAS*, 495, 3065
 Dong-Páez, C. A., Volonteri, M., Beckmann, R. S., et al. 2023, *A&A*, 676, A2
 Dunn, G., Holley-Bockelmann, K., & Bellowary, J. 2020, *ApJ*, 896, 72
 Ellis, J., Fairbairn, M., Hütsi, G., et al. 2023, *A&A*, 676, A38
 Ellis, J., Fairbairn, M., Hütsi, G., et al. 2024, *PhRvD*, 109, L021302
 El-Neaj, Y. A., Alpigiani, C., Amairi-Pyka, S., et al. 2020, *EPJQT*, 7, 6
 Finn, L. S., & Chernoff, D. F. 1993, *PhRvD*, 47, 2198
 Fontanot, F., Monaco, P., & Shankar, F. 2015, *MNRAS*, 453, 4113
 Fragione, G., Loeb, A., Kocsis, B., & Rasio, F. A. 2022, *ApJ*, 933, 170
 Gallo, E., & Sesana, A. 2019, *ApJL*, 883, L18
 Gerosa, D., Ma, S., Wong, K. W. K., et al. 2019, *PhRvD*, 99, 103004
 Girelli, G., Pozzetti, L., Bolzonella, M., et al. 2020, *A&A*, 634, A135
 Greene, J. E., Strader, J., & Ho, L. C. 2020, *ARA&A*, 58, 257
 Haidar, H., Habouzit, M., Volonteri, M., et al. 2022, *MNRAS*, 514, 4912
 Hao, W., Kouwenhoven, M. B. N., Spurzem, R., et al. 2024, *MNRAS*, 527, 10705
 Hartwig, T., Volonteri, M., Bromm, V., et al. 2016, *MNRAS*, 460, L74
 Hogan, J. M., Johnson, D. M. S., Dickerson, S., et al. 2011, *GRGr*, 43, 1953
 Hütsi, G., Raidal, M., Vaskonen, V., & Veermäe, H. 2021, *JCAP*, 03, 068
 Inayoshi, K., Visbal, E., & Kashiyama, K. 2015, *MNRAS*, 453, 1692
 Izquierdo-Villalba, D., Colpi, M., Volonteri, M., et al. 2023, *A&A*, 677, A123
 Kelly, B. C., & Shen, Y. 2013, *ApJ*, 764, 45
 Kormendy, J., & Ho, L. C. 2013, *ARA&A*, 51, 511
 Krolik, J. H., Volonteri, M., Dubois, Y., & Devriendt, J. 2019, *ApJ*, 879, 110
 Lacey, C. G., & Cole, S. 1993, *MNRAS*, 262, 627
 Madau, P., & Rees, M. J. 2001, *ApJL*, 551, L27
 Mandel, I., Farr, W. M., & Gair, J. R. 2019, *MNRAS*, 486, 1086
 Mangiagli, A., Klein, A., Bonetti, M., et al. 2020, *PhRvD*, 102, 084056
 Mayer, L., Kazantzidis, S., Madau, P., et al. 2007, *Sci*, 316, 1874
 Miller, B. P., Gallo, E., Greene, J. E., et al. 2015, *ApJ*, 799, 98
 Natarajan, P. 2021, *MNRAS*, 501, 1413
 Poisson, E., & Will, C. M. 1995, *PhRvD*, 52, 848
 Portegies Zwart, S. F., Baumgardt, H., Hut, P., Makino, J., & McMillan, S. L. W. 2004, *Natur*, 428, 724
 Press, W. H., & Schechter, P. 1974, *ApJ*, 187, 425
 Rasskazov, A., Fragione, G., & Kocsis, B. 2020, *ApJ*, 899, 149
 Reines, A. E. 2022, *NatAs*, 6, 26
 Reines, A. E., & Volonteri, M. 2015, *ApJ*, 813, 82
 Remillard, R. A., & McClintock, J. E. 2006, *ARA&A*, 44, 49
 Ricarte, A., & Natarajan, P. 2018a, *MNRAS*, 474, 1995
 Ricarte, A., & Natarajan, P. 2018b, *MNRAS*, 481, 3278
 Sesana, A., Gair, J., Berti, E., & Volonteri, M. 2011, *PhRvD*, 83, 044036
 Sesana, A., Haardt, F., Madau, P., & Volonteri, M. 2004, *ApJ*, 611, 623
 Tanaka, T. L., & Li, M. 2014, *MNRAS*, 439, 1092
 Treister, E., Schawinski, K., Volonteri, M., & Natarajan, P. 2013, *ApJ*, 778, 130
 Volonteri, M., Habouzit, M., & Colpi, M. 2021, *NatRP*, 3, 732
 Volonteri, M., Lodato, G., & Natarajan, P. 2008, *MNRAS*, 383, 1079
 Volonteri, M., Pfister, H., Beckmann, R. S., et al. 2020, *MNRAS*, 498, 2219
 Wang, H.-T., Jiang, Z., Sesana, A., et al. 2019, *PhRvD*, 100, 043003
 Xu, H., Chen, S., Guo, Y., et al. 2023, *RAA*, 23, 075024
 Zic, A., Reardon, D. J., Kapur, A., et al. 2023, *PASA*, 40, e049